An RF-Powered Temperature Sensor Designed for Biomedical Applications

Gustavo Campos Martins and Fernando Rangel de Sousa
Department of Electrical Engineering, Federal University of Santa Catarina, Florianópolis, Brazil
Email: {gustavocm, rangel}@ieee.org

***Abstract*—An RF-powered temperature sensor with power management and communication circuits designed with a standard $130\,\mathrm{nm}$ CMOS technology is reported. The system was designed to have an RFID-like functionality, i.e., the device communicates with an external reader, receiving power and backscattering information. Initially, the system collects energy in a low-power charging mode, with a rectifier optimally designed to operate with signal levels as low as $-10\,\mathrm{dBm}$ centered approximately $900\,\mathrm{MHz}$. Operating at condition of minimum input power, the system takes around $70\,\mu\mathrm{s}$ to power up. A calibration method was designed to enable a measurement error of less than $0.1\,^{\circ}\mathrm{C}$ while the sensor operates in the human body temperature range (35 to $42\,^{\circ}\mathrm{C}$). The circuits were simulated in the Cadence Spectre environment and the total power consumption observed was approximately $8.5\,\mu\mathrm{W}$ when in active mode and $4.9\,\mu\mathrm{W}$ when in standby mode. Some parts of the circuit were measured and preliminary results are reported.**

I. Introduction

The evolution in integrated circuits technology and circuit design techniques is enabling the development of more efficient, safe, reliable and cheap biomedical electronic devices. With this evolution, such devices started appearing inside commercial products, such as pacemakers [1] and cochlear implants [2]. Biomedical electronics is a promising field and may reduce cost in many other kinds of expensive treatments. For example, the annual cost of neurological treatments is over US$500 billion and is expected to grow as the population ages [3]. Innovative biomedical devices can reduce these costs while producing better results, but we still have to overcome several challenges to allow mass adoption of such devices.

A challenge in the design of biomedical electronics is power management and power transfer or harvesting. This challenge is even greater in implanted devices, which are not physically accessible without a surgery. Even in devices that are not implanted (on-body), it is convenient to have a remote means of charging a battery or just powering a batteryless system. To solve this problem, many kinds of energy harvesting techniques have been devised, such as harvesting from temperature differences, mechanical oscillations, pH differences, radio frequency (RF) signals, among other energy sources [4], [5]. In this paper we present a system that uses an RF signal to power a temperature sensor for on-body temperature monitoring.

Our system is based on the basic functionality of a fully-passive RFID tag. In which the input signal, which powers the tag, is provided by a reader and the communication with the reader happens through the modulation of the reflected signal, using a backscattering modulation. A block diagram of the implemented system is presented in Fig. 1.

The system presented in this paper was designed with a standard $130\,\mathrm{nm}$ CMOS technology. In the next session, its architecture is presented along with its operating principles. The RF and Analog circuits designed for this system are discussed in Sections III and IV, respectively. In Section V, the system is simulated as a whole to validate the designs and some block measurements are presented. Finally, the work conclusions are presented in the last section.

II. System Architecture

The blocks shown in Fig. 1 can be divided in two groups: RF front end and analog circuits. The goals of the RF front end are to collect energy from the RF signal and to transmit data to the reader. These tasks are performed by the rectifier, impedance matching and backscattering modulator. The remaining blocks are the analog circuits, which manage the stored energy and measure the temperature, generating the input to the backscattering modulator.

The maximum power transfer from the antenna to the rectifier will be guaranteed by the impedance matching network when the impedance of the backscattering device is high, as we will discuss later. The rectifier generates a DC voltage at its output, charging a capacitor large enough to supply energy to the system when the signal is not available at the rectifier input. This happens when the backscattering device is conducting current (low impedance) and the signal is reflected back to the reader. Information about the measured temperature is contained in the frequency of the OOK (On-Off keying) modulation of the reflected signal.

A voltage limiter is attached to the rectifier output to limit the voltage to $1.2\,\mathrm{V}$, which is the highest supply voltage supported by this technology. The next block is the mode selector, which senses the voltage over C_S and switches on or off other blocks, through the signal V_{ctr}, depending on the energy stored in C_S. At the moment the voltage reaches certain threshold value, the voltage regulator starts operating to stabilize the sensor's supply voltage. The mode selector also starts the ring oscillator, which is biased with a current related to I_{ref} generated in the reference source. The reference source is the temperature-sensitive device and it also generates a voltage reference V_{ref} for the voltage regulator and mode

978-1-4799-1132-5/13/$31.00

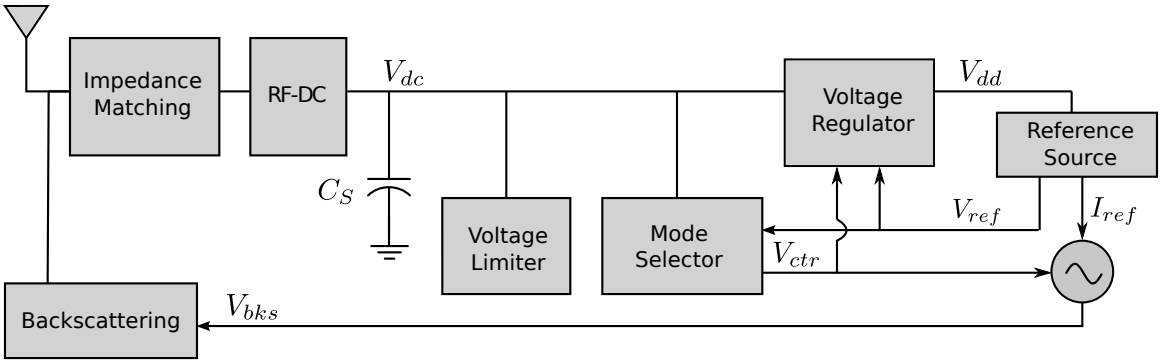

Fig. 1. System block diagram

selector blocks. Using its current to bias the oscillator we generate a signal that has temperature-dependent frequency.

III. RF Front End

To elaborate the RF front end specifications, we considered that the reader would be similar to the one presented in [6]. This reader has sensitivity equal to $-61\,\mathrm{dBm}$, output power up to $33\,\mathrm{dBm}$ and antenna gain of $7.8\,\mathrm{dBi}$. We didn't design the antenna for this device, so we considered the typical dipole antenna gain for antennas used in RFID, which is approximately $2\,\mathrm{dBi}$ [7]. To calculate the minimum power of the input signal we used the Friis transmission equation [8] with the presented specifications and the backscattering device loss (which will be presented later). Choosing the signal frequency equal to $900\,\mathrm{MHz}$, the calculated value is approximately $-10\,\mathrm{dBm}$. So, we chose this as the worst-case specifications for the input signal, which was used to design the circuits presented in this section

A. Backscattering

This device is responsible for sending information to the reader. It consists in an NMOS transistor in parallel with the matching network, the transistor M_1 shown in Fig. 2. To send information to the reader it changes the input impedance, matching or mismatching it to the antenna impedance. When the impedance is matched, $Z_{in} \approx 50\,\Omega$, there is no reflection and when it is mismatched, $Z_{in} \approx 0\,\Omega$, the signal is reflected back to the reader. If the reader can sense this reflected signal, it can receive data from the sensor.

To design the transistor M_1, we used $L = L_{min}$ and, through simulation, we found which value of W provided a reasonable difference between the reflections in matched and mismatched states. We chose a value of $50\,\mu\mathrm{m}$ for W.

The reflection coefficient (S11) versus V_{bks} for the chosen geometry of M_1 is presented in Fig. 3. In this case there is a difference of nearly $35\,\mathrm{dB}$ between the two states. At the worst-case specifications for the input signal, the reader can sense only the reflected signal when V_{bks} is high.

B. Rectifier

The implemented rectifier is shown in Fig. 4 and has 16 stages. The circuit of each stage is based on the Greinacher

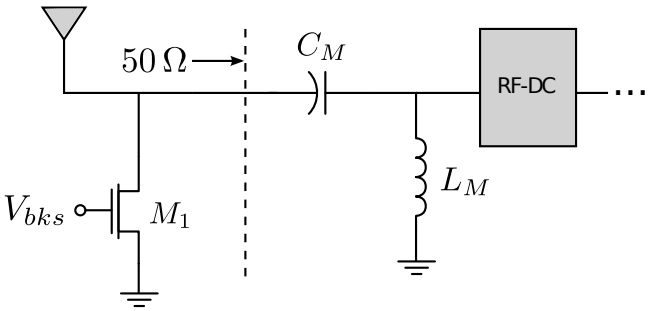

Fig. 2. Matching network and OOK backscatter modulator schematics

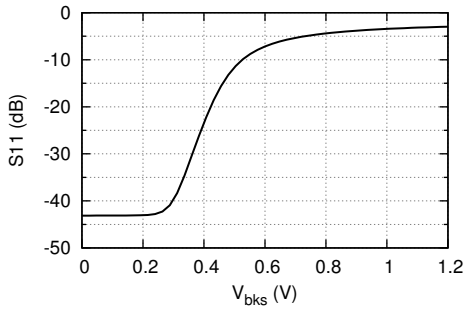

Fig. 3. Reflection versus gate voltage V_{bks} with an ideal $50\,\Omega$ load representing the system input impedance

voltage doubler with each diode implemented with a native transistor configured as diode. This block was developed considering a $10\,\mu\mathrm{A}$ current load at its output. The efficiency of the rectifier, which is the relationship between the output DC power and the power available at the input of the impedance matching block (P_{out}/P_{av}), is 10% with the worst-case input.

The supply capacitor C_S was designed to provide autonomy to the system while operating. Its capacitance must be high enough to allow the system to operate while V_{bks} is high, i.e., while the power is reflected and doesn't enter the rectifier. The value we chose for this capacitor was $200\,\mathrm{pF}$, which provides an autonomy for 16 cycles of V_{bks} ($27\,\mu\mathrm{s}$) with worst-case input at $38.5\,^{\circ}\mathrm{C}$ (center of temperature range).

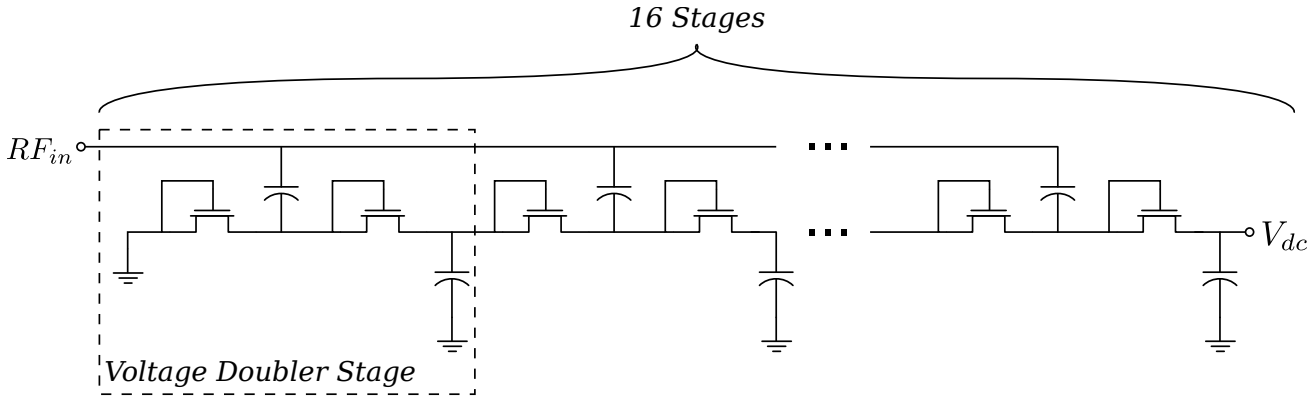

Fig. 4. Rectifier circuit schematics

C. Impedance Matching

The simulated rectifier input impedance, with output voltage equal to $1.2\,\mathrm{V}$ and input power $-10\,\mathrm{dBm}$, is equal to $219 - 291j\,\Omega$. We matched this impedance to $50\,\Omega$ to allow maximum power transfer when using our $50\,\Omega$-based test setup. For this we used an L-match circuit [9], with a shunt inductor L_M and a series capacitor C_M as shown in Fig. 2.

For effectively designing the matching, several iterations were needed. Each iteration consisted in designing the matching network schematics to match $50\,\Omega$, doing the layout, extracting the parasitic from the layout, reevaluating the impedance considering the parasitics and redesigning the impedance matching again. This is necessary because parasitics have non-negligible influence on the input impedance, because the routing becomes large. We obtained the values $C_M = 1.68\,\mathrm{pF}$ and $L_M = 12\,\mathrm{nH}$ after this process. We used integrated inductor and capacitor in this design.

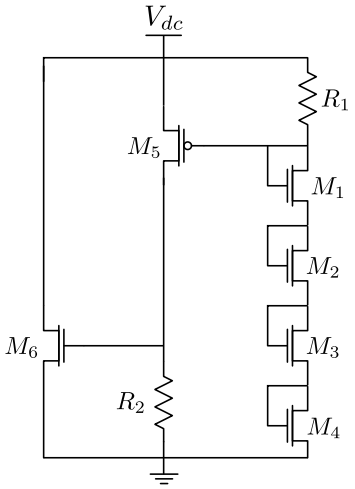

Fig. 5. Voltage limiter schematics

IV. Analog Circuits

The analog circuits are responsible for generating the backscattering input signal, a temperature-dependent signal. As we discussed in the last section, at the worst-case input the output power is $10\,\mu\mathrm{W}$, which we consider to be the maximum power consumption of the rest of the system. So, we designed the analog circuits with this power budget in mind.

A. Voltage Limiter

For the CMOS technology used in this project, the maximum supply voltage is $1.2\,\mathrm{V}$. This circuit clamps the supply voltage by consuming a large current when it get over $1.2\,\mathrm{V}$. A circuit based on the limiter presented in [10] was designed, see Fig. 5. The simulation and measurement results of this circuit are discussed in Section V.

B. Mode Selector

This circuit monitors the supply voltage and enables the voltage regulator and the oscillator. When the output of the mode selector is low, it means that the system is in standby mode and when it approaches V_{dd} the mode selector activates the system. This block was designed to make sure that the sensor will produce an output only if the V_{dc} is high enough, i.e., if the capacitor C_S has energy enough and the sensor will be able to produce the correct output. This block also allows a low power consumption during the charging stage.

If the rectifier output power is low (but still higher than than the standby power consumption), the capacitor C_S is charged. When supply voltage reaches a value V_{on} the mode selector will enable the rest of the system and more current will be draw from C_S, lowering the supply voltage until it reaches V_{off}. Then the mode selector will disable the blocks allowing V_{dc} to rise again. To guarantee the correct operation of the sensor, V_{off} must be greater than the start-up voltage of the reference generator.

This characteristic is obtained from the hysteresis comparator shown in Fig. 6, which was designed based on [11]. The input signals are generated by the reference source's node V_{ref} (inverting input) and a circuit biased by the reference V_{slope} (non-inverting input), see Fig. 7(a). In Fig. 7(b) we can observe the hysteresis of the mode selector output, in which the arrows indicate the curve in which V_{DD} is going from low to high or vice-versa. In the typical case $V_{on} = 1.05\,\mathrm{V}$ and $V_{off} = 0.7\,\mathrm{V}$.

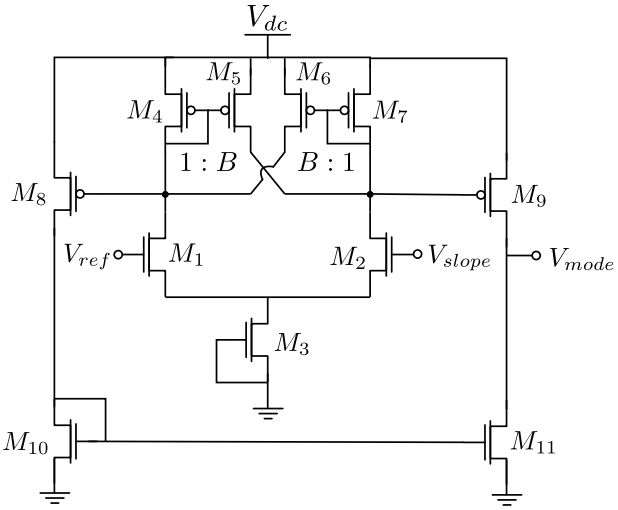

Fig. 6. Mode selector schematics

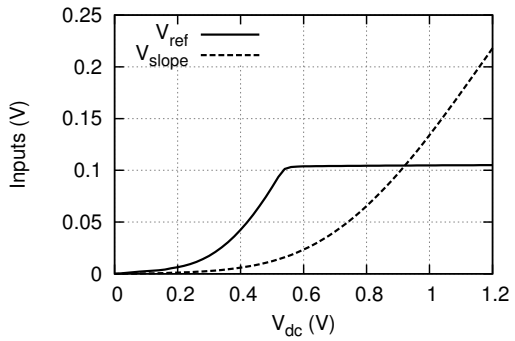

(a)

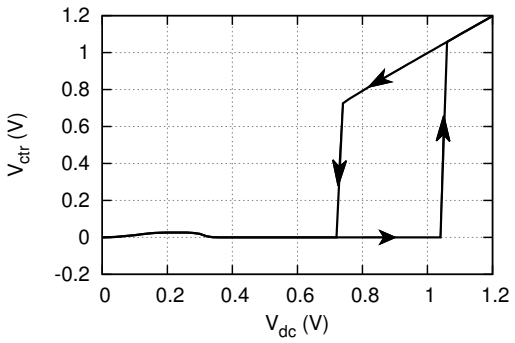

(b)

Fig. 7. Mode selector's typical (a) inputs and (b) outputs (hysteresis indicated by arrows)

Transistor M_3, operating in the subthreshold regime, provides a low bias current to the comparator. This circuit consumes $34\,\mathrm{nA}$ at $1\,\mathrm{V}$ supply. Monte Carlo simulations of this circuit and reference generator were performed to make sure that V_{off} is always high than the minimum operating V_{dd} voltage of the reference generator.

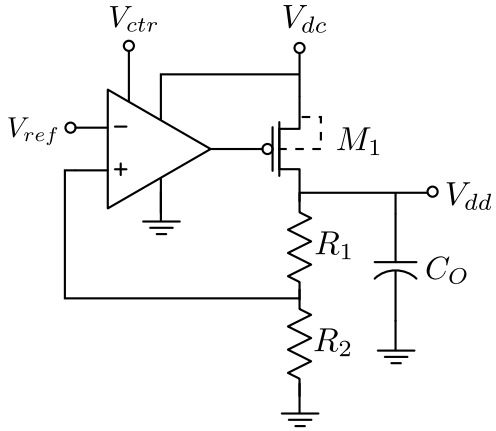

Fig. 8. LDO regulator simplified schematics

C. Voltage Regulator

A voltage regulator is used in this system because the changes of V_{dd} during the sensor operations cannot be neglected. Although the voltage reference has relatively low power supply sensitivity, it is still not low enough and the variations that occur in supply voltage (tenths of a V) are enough to cause considerable errors on the temperature reading (tenths of a $^{\circ}\mathrm{C}$).

A Low-Dropout (LDO) voltage regulator was implemented. Its simplified schematics is presented in Fig. 8. The OpAmp is enabled or disabled by the mode selector. When enabled, this block presents $3\,\mu\mathrm{A}$ current consumption and regulates V_{dd} to a value equal to $7V_{ref}$, which is approximately $0.8\,\mathrm{V}$. The inputs of the OpAmp are V_{ref} and voltage created through the feedback composed by $R_1 = 3\,\mathrm{M\Omega}$ and $R_2 = 500\,\mathrm{k\Omega}$. When disabled, the OpAmp output is equal to ground voltage, letting current flows through the pass transistor M_1, which has $L = 0.5\,\mu\mathrm{m}$ and $W = 4\,\mu\mathrm{m}$. The output capacitor C_O has $50\,\mathrm{pF}$ and was sized to stabilize the regulator output.

D. Temperature Sensor

The temperature-sensitive device of the system is the threshold-based current reference generator [12] presented in Fig. 9, composed by transistors M_3-M_8 and R_1. The current starved ring oscillator, represented in the figure as block with output V_{bks}, is composed by 5 inverters. Another inverter is placed at its output to shift the peak-to-peak voltage of the signal to V_{dc}. We do this to set a sufficiently high at the backscattering input to allow signal reflection. In Fig. 3, we can see that V_{bks} must have at least $0.6\,\mathrm{V}$ peak-to-peak voltage. The oscillator has bias current mirrored from the reference generator by transistors M_1-M_2. The output of the level shifter is connected to the backscattering modulator to generate the sensor output. The mode selector controls whether the oscillator is working or not by controlling the transistor M_9.

The transistors M_{10}-M_{14} and resistor R_2 generates a voltage that is used as a mode selector input. It is initially lower than V_{ref} and later becomes greater than it. It happens

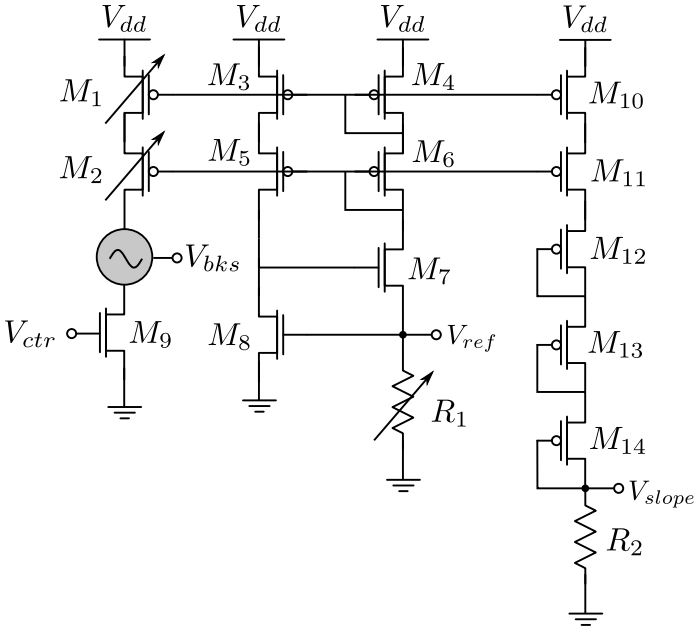

Fig. 9. Temperature sensor (voltage/current reference and oscillator) and voltage slope generator used as the mode selector input

because V_{slope} is related to V_{ref} through a current mirror, the transistors in diode configuration limits the current initially and the resistor R_2 is greater than R_1. The DC simulation results of V_{ref} and V_{slope} are shown in Fig. 7(a).

The circuit presents $I_{bias} = 992\,\mathrm{nA}$ and $I_{ref} = 612\,\mathrm{nA}$ at $38.5\,^{\circ}\mathrm{C}$ (center of temperature range) and $1\,\mathrm{V}$ supply voltage. At this operating conditions, the power consumption of this circuit (including the oscillator and voltage slope branches) is $2.8\,\mu\mathrm{W}$ while the oscillator is functioning, the oscillator output presents $-0.78\,\%/^{\circ}\mathrm{C}$ temperature coefficient (TC), $660\,\mathrm{kHz}$ frequency and $2.37\,\%/\mathrm{V}$ sensitivity to power supply.

Both R_1 and M_1-M_2 can be calibrated to fit the output signal frequency versus temperature curve to the nominal one. The variable resistor R_1 is made of 8 series scaled resistors (high resistive polysilicon), that be can short-circuited, and it calibrates the output TC. The variable current mirror $M_1 - M_2$ is composed by 13 parallel scaled transistors that calibrates the current level while (ideally) maintaining the TC. We designed these devices to be possible to calibrate the circuit to achieve less than $0.1\,^{\circ}\mathrm{C}$ measurement error. Monte Carlo simulations were performed to specify the ranges and minimum step needed for the variable devices.

V. Validation

A transient simulation of the analog circuits was performed using a $10\,\mu\mathrm{A}$ ideal current source representing the rectifier output current with $-10\,\mathrm{dBm}$ input power. Some of the generated signals are presented in Fig. 10. After $50\,\mu\mathrm{s}$ of receiving power from the source, the mode selector starts the voltage regulator and oscillator. Before this, while the V_{ctr} is low, V_{dd} follows V_{dc}. After another $20\,\mu\mathrm{s}$, the oscillator

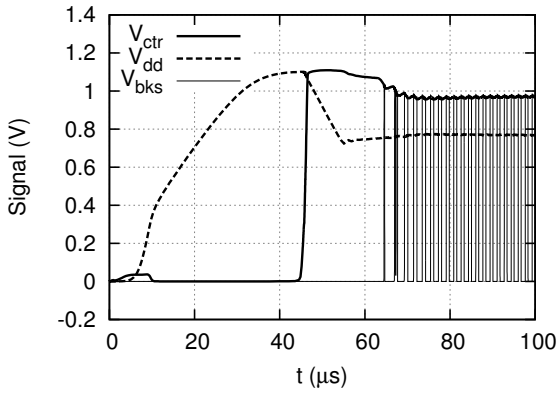

Fig. 10. Temperature system transient simulation

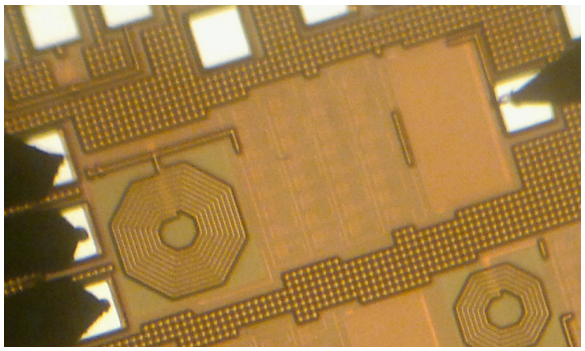

Fig. 11. Rectifier photograph during tests

starts and generates the correct output signal. The peak-to-peak voltage of V_{bks} is equal to V_{dc}.

We sent a first chip to fabrication, which contained the rectifier and voltage limiter designs. It returned from fabrication and the circuits were tested. Fig. 11 shows a photograph of the rectifier (with C_S capacitor) during tests. On the left is the input RF probe and on the right the DC output. For testing the rectifier, we placed a $100\,\mathrm{k}\Omega$ load at its output to provide a $10\,\mu\mathrm{A}$ load current at $1\,\mathrm{V}$ output voltage. With minimum input power condition, the S11 at $900\,\mathrm{MHz}$ was $-15\,\mathrm{dB}$ and efficiency approximately 10%. The voltage limiter current consumption at $1\,\mathrm{V}$ is $2\,\mu\mathrm{A}$. In Fig. 12, we show the measurement and simulation results of the limiter current consumption. The measurement results were close to the expected.

VI. Conclusion

We designed an RF-powered temperature sensor suitable for human body temperature measurements using a standard $130\,\mathrm{nm}$ CMOS technology. The system operates in two modes: standby and active. In active mode the system consumes $8.5\,\mu\mathrm{A}$ and in standby mode it consumes $4.9\,\mu\mathrm{A}$, with $1\,\mathrm{V}$ supply voltage and $38.5\,^{\circ}\mathrm{C}$. With the minimum input signal specification, the rectifier works with 10% efficiency providing $10\,\mu\mathrm{A}$ output current. The active area of the final layout is approximately $0.34\,\mathrm{mm}^2$. The largest layout is the rectifier block one ($0.26\,\mathrm{mm}^2$), which includes an inductor and the

TABLE I
COMPARISON WITH RECENT WORKS

Reference	[13]	[14]	[15]	[16]	[17]	This Work
Technology (nm)	250	130	130	130	180	130
Input Frequency (MHz)	450	900	900	868	910	900
Area (mm^2)	1.2	-	0.95	3.96	1.2	0.34
Standby power consumption (μW)	5	6	-	≈ 0.11	-	4.9
Active power consumption (μW)	1500	9	7.9	-	7	8.5
RF-DC Efficiency (%)	-	30*	8.6	35*	-	10
Minimum input power (dBm)	-12.5	-12	-10.3	-	-5	-10

* Efficiency is not defined in these papers. Since some papers consider efficiency as voltage conversion efficiency not power, we cannot stablish a clear comparison.

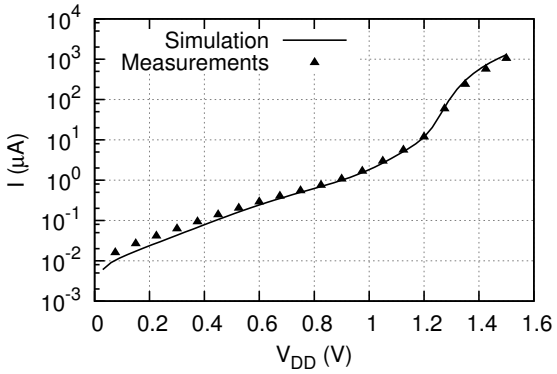

Fig. 12. Limiter's measured and simulated current consumption

storage capacitor. The sensor has a temperature coefficient of $-0.78\,\%/^{\circ}\mathrm{C}$ and designed to have maximum measurement error, after calibration, of $0.1\,^{\circ}\mathrm{C}$.

In Table I we compare our work to recent RF-powered temperature sensors, developed with similar technology and input signal frequency. We developed a low power system that works with low input power. Regarding the energy conversion efficiency, the circuits of [14] and [16] achieve high efficiency with low input power, but they do not define what is efficiency for them. Since sometimes efficiency is defined by the relation output and input voltage levels (not power), we cannot assert whether our system achieves better results than theirs at this aspect. We managed to develop a system that occupies a very small area, if compared to the others, while having the capabilities of calibration. The calibration circuits occupied a large area of the circuit, but the dominant devices were still the inductor (in matching) and storage capacitor C_S.

All the blocks presented in this paper were sent to fabrication. Further works consist in testing the rest of the circuits and in testing the complete system, with all the blocks connected.

ACKNOWLEDGMENT

We would like to thank CNPq for the student scholarship and MOSIS for chip fabrication. We thank Davi Luciano Figueiredo and Luccas Meller Casagrande for the help with layout design and to Paulo Márcio Moreira e Silva for the help with testing the rectifier.

REFERENCES

[1] MEDTRONIC, "Pacemakers — Pacemakers for Bradyarrhythmia Management." [Online]. Available: http://www.medtronic.com/for-healthcare-professionals/products-therapies/cardiac-rhythm/pacemakers/index.htm

[2] A. BIONICS, "Products — advanced bionics." [Online]. Available: http://www.advancedbionics.com/com/en/products.html

[3] Society for Neuroscience, *Brain facts: a primer on the brain and nervous system*. Society for Neuroscience, 2012.

[4] S. Kamel Tabbakh, R. Maarefdoust, N. C. Kyun, and B. Mohd Ali, "Environmental taxonomy of power scavenging techniques for autonomous self powered wireless sensors," in *Circuits and Systems (APCCAS), 2010 IEEE Asia Pacific Conference on*, dec. 2010, pp. 1031 –1034.

[5] R. Vullers, R. Schaijk, H. Visser, J. Penders, and C. Hoof, "Energy harvesting for autonomous wireless sensor networks," *Solid-State Circuits Magazine, IEEE*, vol. 2, no. 2, pp. 29 –38, spring 2010.

[6] I. Mayordomo, R. Berenguer, A. Garcia-Alonso, I. Fernandez, and I. Gutierrez, "Design and implementation of a long-range rfid reader for passive transponders," *Microwave Theory and Techniques, IEEE Transactions on*, vol. 57, no. 5, pp. 1283–1290, 2009.

[7] K. Finkenzeller, *RFID handbook: fundamentals and applications in contactless smart cards, radio frequency identification and near-field communication*. Wiley, 2010.

[8] H. T. Friis, "A note on a simple transmission formula," *proc. IRE*, vol. 34, no. 5, pp. 254–256, 1946.

[9] T. H. Lee, *The design of CMOS radio-frequency integrated circuits*. Cambridge university press, 2003.

[10] U. Kaiser and W. Steinhagen, "A low-power transponder ic for high-performance identification systems," *Solid-State Circuits, IEEE Journal of*, vol. 30, no. 3, pp. 306–310, 1995.

[11] P. E. Allen and D. R. Holberg, *CMOS analog circuit design*. Holt, Rinehart and Winston New York, 1987.

[12] P. R. Gray, P. J. Hurst, R. G. Meyer, and S. H. Lewis, *Analysis and design of analog integrated circuits*. John Wiley & Sons, 2008.

[13] F. Kocer and M. Flynn, "An rf-powered, wireless cmos temperature sensor," *Sensors Journal, IEEE*, vol. 6, no. 3, pp. 557 –564, june 2006.

[14] D. Yeager, F. Zhang, A. Zarrasvand, N. George, T. Daniel, and B. Otis, "A 9 μA, Addressable Gen2 Sensor Tag for Biosignal Acquisition," *Solid-State Circuits, IEEE Journal of*, vol. 45, no. 10, pp. 2198 –2209, oct. 2010.

[15] H. Reinisch, M. Wiessflecker, S. Gruber, H. Unterassinger, G. Hofer, M. Klamminger, W. Pribyl, and G. Holweg, "A multifrequency passive sensing tag with on-chip temperature sensor and off-chip sensor interface using epc hf and uhf rfid technology," *Solid-State Circuits, IEEE Journal of*, vol. 46, no. 12, pp. 3075 –3088, dec. 2011.

[16] A. Vaz, A. Ubarretxena, I. Zalbide, D. Pardo, H. Solar, A. Garcia-Alonso, and R. Berenguer, "Full passive uhf tag with a temperature sensor suitable for human body temperature monitoring," *Circuits and Systems II: Express Briefs, IEEE Transactions on*, vol. 57, no. 2, pp. 95 –99, feb. 2010.

[17] J. Qian, C. Zhang, L. Wu, X. Zhao, D. Wei, Z. Jiang, and Y. He, "A passive UHF tag for RFID-based train axle temperature measurement system," in *Custom Integrated Circuits Conference (CICC), 2011 IEEE*, sept. 2011, pp. 1 –4.